INTERNATIONAL ATOMIC ENERGY AGENCY
UNITED NATIONS EDUCATIONAL, SCIENTIFIC AND CULTURAL ORGANIZATION

INTERNATIONAL CENTRE FOR THEORETICAL PHYSICS
34100 TRIESTE (ITALY) - P.O.B. 586 - MIRAMARE - STRADA COSTIERA 11 - TELEPHONE: 2240-1
CABLE: CENTRATOM - TELEX 460392-I

H4.SMR.203 - 35

" SPRING COLLEGE ON GEOMAGNETISM AND AERONOMY "

(2 - 27 March 1987)

" Magneto - variational studies " - II

presented by :

B.P. SINGH
Indian Institute of Geomagnetism
Dr. Nanabhoy Moos Road
Colaba
Bombay 400 005
India

Lecture - IV

Topics:

(i) Perturbation Arrows
(ii) Hypothetical Event Analysis (HEA)
(iii) Effect of Source Field Geometry
(iv) Observational Results from Indian Region
(v) Global Conductivity Distribution

(i) Perturbation Arrows

(Ref: B.R. Arora: Perturbation arrows and hypothetical event analysis in geomagnetic induction studies: experimental results from north-west India: to appear in Physics of Earth and Planetary Interiors)

The induction arrows (also called Parkinson or Wiese vectors), point at right angles to the internal concentrations of current ~~flow~~ and have been used widely to locate the conductive zones. The perturbation arrows, to be defined later, provide both the strength and direction and strength of the anomalous induced currents. They help to visualise the intensity and geometrical configuration of an underground conductivity anomaly. Despite their clear physical significance, perturbation arrows have scarcely been used in geomagnetic studies.

As a consequence of the linearity of Maxwell's equations, there exists a linear relationship between the Fourier transforms of the anomalous and the normal field components. The normal component is defined as the sum of contributions from the external current and that part of the internal current which is generated in a spherically symmetric conductive structure of the Earth. The anomalous field is considered as being due to ~~the~~ none-one-dimensional conducting structures, and is entirely internal in origin. The quasi-uniform nature of the external field further presumes that the normal part of the vertical field (Z_n) will be small. Under these circumstances, the relation between the Fourier transform of the anomalous and the normal field at a particular frequency can be expressed as:

$$X_a = T_{xx} X_n + T_{xy} Y_n$$

$$Y_a = T_{yx} X_n + T_{yy} Y_n$$

$$Z_a = T_{zx} X_n + T_{zy} Y_n$$

In the above equations T's are the transfer functions. One could note that $T_{zx} = A$ and $T_{zy} = B$ of the earlier lecture. The subscripts 'a' and 'n' refer to anomalous and normal parts, respectively. The transfer functions contain information about the nature of the internal field anomaly. The observed value at a station

$$X = X_a + X_n$$

and to A is true for Y and Z. We assume

that observed Z is usually Za i.e. ($Z_n \simeq 0$). To separate the X and Y records in their normal and anomalous parts use is made of simultaneous records from a normal station in the surveyed area. The criterion for identifying a normal station is that first ~~Z=0~~ Z-variation should be zero there. Since Z-variations could also be zero over a conductor, it should also be checked that X and Y variations have no enhancement there. Once, such a station is identified, its variations of X and Y are subtracted from data of other field stations to get X_a and Y_a at each of them.

The transfer functions (T's) are calculated by making a least squares fit to say a measurement set of six or more independent events. Taking $\vec{i}$ and $\vec{j}$ as unit vectors in north (x) and east (y) directions the induction arrow for a particular frequency is defined as:

$$\vec{I}_{real} = -\mathrm{Re}[T_{xx}]\vec{i} - \mathrm{Re}[T_{xy}]\vec{j}$$

(in-phase arrow)

$$\vec{I}_{imag} = -\mathrm{Im}[T_{xx}]\vec{i} - \mathrm{Im}[T_{xy}]\vec{j}$$

(quadrature-arrow)

In this notation, arrows point towards mineral current concentration and are used to define the strike of conductivity

anomaly. The complex perturbation arrows $\vec{P}$ and $\vec{Q}$ are defined as:

$$\vec{P} = -T_{xx}\vec{i} - T_{yx}\vec{j}$$

$$\vec{Q} = T_{xy}\vec{i} + T_{yy}\vec{j}$$

for both real and quadrature arrows. The resultant of $\vec{P}+\vec{Q}$ is rotated 90° anticlockwise to indicate the strength and direction of anomalous mineral ~~fields~~ current. This current flow is superposed on the flow of unperturbed normal currents.

One set of induction and perturbation vectors from the north-west Indian array data is shown in Fig. 1. The $\vec{P}+\vec{Q}$ arrows show the overall pattern of anomalous current flow. In general, it is noticed that $\vec{P}+\vec{Q}$ arrows are oriented at right angles to the induction arrows. Both real and quadrature $\vec{P}+\vec{Q}$ arrows ~~follow~~ are largest in between oppositely directed real induction arrows. This is in conformity with the postulation that such zones are areas of current concentration. From the trend in the rate of decrease of ~~real~~ perturbation arrow strength, it was estimated that the horizontal half-width of the main conducting zone could be about 100 km.

(iii) Hypothetical Event Analysis (HEA)

In this approach synthesized Fourier amplitude and phase maps are prepared with the transfer functions calculated in the last section. Say the anomaly in Z can be calculated through the relation

$$Z_a = T_{zx} X_n + T_{zy} Y_n$$

using the values for T ~~est~~ estimated at the station and taking for X_n and Y_n some known values. Advantage of this approach is that we can estimate Z_a for any polarization of the source field with proper choice of X_n and Y_n. This way one can accentuate the effect related to strike of the conductor. Other important advantage of hypothetical event technique is that source effect can be totally ~~e~~ eliminated. Whatever contributions were there from the source effect had been eliminated while estimating the T's in the least squares approach. Thus, the Fourier map from hypothetical event is one for a uniform source field. Above all the main advantage of this approach is that one need not operate the whole array simultaneously. Even with five or six magnetometers, through these repeated deployment results can be synthesized for a situation ~~as if~~ as if twenty-to twenty-four stations were operating simultaneously.

Two sets of maps for periods 91 min and 41 min are given in Figs. 2 and 3. In upper panel are shown the maps which were actually observed with the array data. The lower panels are the ones that have been generated by HEA. It has been observed that the polarization for HEA is same as of the midway field for the upper panel. The absolute values are different in the two cases as the HEA plots are for ~~the incident wave~~ a polarized field of unit amplitude. In the plots we also

$$P_{amp} = \sqrt{X_{amp}^2 + Y_{amp}^2}$$

P_{amp} represents the total strength of the horizontal field fluctuations.

In Figs. 2 and 3, the compiled anomalous maps show an anomaly pattern much like the Fourier transform (FT) parameter maps. Stations characterized by high values on the amplitude maps of X- and Y- components are well brought out as centres of concentrated currents on compiled maps. A great deal of similarity ~~was~~ between P_{amp} and P_a maps provides confidence in the physical significance of the perturbation arrows. Vertical field anomaly maps obtained by the two approaches reveal identical anomaly patterns. Broad agreement of FT and HEA generated anomaly maps provides experimental support to suggestion that HEA could be construed as a reliable approach.

(iii) Effect of Source Field Geometry

In the Tikhonov-Cagniard method of magnetotelluric (MT) sounding, which assumes plane electromagnetic wave normally incident on plane-layered earth with conductivity varying as function of depth, the horizontal component of electric field (E_y) and magnetic field (H_x) are related as

$$-E_y = \eta H_x ;$$

where η is the Tikhonov-Cagniard impedance. The subscripts x and y refer to the northerly and easterly directions. It was shown by Wait that in the case of non-uniform incident electromagnetic wave, the relation between orthogonal electric and magnetic field components is modified and can be expressed as

$$-E_y = \eta H_x + \frac{\eta}{2\gamma^2}\left(\frac{\partial^2 H_x}{\partial x^2} + \frac{\partial^2 H_x}{\partial y^2} + \frac{\partial^2 H_x}{\partial x \partial y}\right).$$

The parameters η & γ defined in SI units as:

$$\eta^2 = \frac{i\omega\mu_0}{\sigma} \quad \text{and} \quad \gamma^2 = i\omega\mu_0\sigma.$$

In the above equations the time dependence of the field has been taken as $e^{i\omega t}$. Implicating that a deviation of E_y/H_x from Tikhonov-Cagniard equation is associated with the second spatial derivative of horizontal field, Dimitriev and Berdichevsky in 1975 showed that general one-dimensional Tikhonov-Cagniard model is the linearity of the horizontal field rather than the sources of these changes. Thus one finds that only where the second derivative of source field is non-zero the Cagniard-Tikhonov equation becomes questionable. As such a situation arises under the centre of equatorial and auroral electrojets, these particular cases have to be applied in MT surveys. So far no observational finding has been reported to establish the modifications suggested in Tikhonov-Cagniard equation. In its regard observations from the array operated under equatorial electrojet in India are of inbuilt and the findings so obtained therefrom are discussed below to bring out the validity of Wait's suggestions.

In the earlier lectures, it has been mentioned that the source field effect is dependent critically on the parameter λ ($= \sigma\mu\omega/\gamma^2$). As λ decreases, the inductivity of induced current also decreases. A small λ means, a source of large wave number or small wavelength i.e. a highly non-uniform source. Further, the source field effect is strongly dependent on σ and ω. Even a non-uniform source can induce significant current when either or both of σ and ω

are large This dependence of current induced by a localized source on σ, the conductivity of sub-surface layers, is apparent when one sees the electrojet profiles in Fig. 4. The equatorial electrojet variations are very different from region to region The figure is taken from the book on GDS written by Rokityansky. The author suggests that one could visualize the source field effect as geometric attenuation of the wave as it propagates. A diverging wave besides the usual attenuation from the current it induces, will also get attenuated from geometrical spreading. He puts a limit of 250 km as depth of investigation by equatorial electrojet and as 430 km by auroral electrojet. Though such a depth limit may signify that GDS under electrojet is of little use, it has another advantage that it makes the problem well posed

Non-uniform source fields can be of help in estimating depth-conductivity profiles through GDS in 1-D cases which otherwise is not possible. The application of this approach would be taken below

(IV) Observational Results from Indian Region

The Southern tip of India is a region which is under the influence of a non-uniform source field in the day-time and a uniform source field in the night-time. This

region surrounded by sea on three sides and separated from Sri Lanka Island by a narrow Palk Strait introduces large perturbations in the flow of induced currents. The presence of a conducting channel underneath Palk Strait in the lower crust or upper mantle further accentuates the induction effects on surface geomagnetic variations.

A magnetic array was operated in this region in 1975-1980. The data collected during this survey has been used by Sharmila Ranjit et al. (1986) to discern source-field field effects on the estimates of current induced. The observational network is given in Fig 5. The locations of eleven stations whose data were used in analysis are shown in Fig. 5. by filled circles. Forty hours of variations corresponding to magnetic storm of Feb 6-7, 1980 were digitized and stacked plots are shown in Figs. 6. The plots of H-variations show a family consistent form over the entire array. However, related Z-variations show marked differences, both in form and amplitude. Realizing that the induction effects are frequency dependent, comparison of features needs to be done in frequency domain. A direct comparison of FT amplitudes and phases will be of limited use since the FT spectrum integrates over both the day- and night-time events. To see the night and day

features separately, the technique of complex demodulation was adopted. This method gives the variation with time of the amplitude and phase of the selected frequency. As the Fourier spectrum of the event showed two pronounced peaks around the periods of 110 and 54 min, demodulates were obtained for period midrange 171-82 min and 64-46 min. The resultant amplitudes variations in the demodulated series corresponding to the period band of 171-82 min are given in Fig. 7. The demodulates show substantially large amplitudes close to 19 hr LT on Feb 6, 1980 and 11 LT on Feb 7, 1980. The H-amplitudes of peak around 11 LT show an increasing trend towards the dip equator. This enhancement can be understood in terms of the influence of the concentration of ionospheric currents along the dip equator. A suppression of H-amplitudes is seen near the dip equator for the night-time event around 19 hr LT. This is related to induction effects in the region. The night-time Z-variations are non-zero at all stations except G3, on the contrary the day-time Z-variations are zero for all but the B2, B3, C2 & D4. By making a detailed analysis Banerjee Rangaji et al. (1984) have shown that the intensity of induced currents gets weakened when inducing field is uniform and this weakening is limited to zones with

non-zero second derivative (spatial) of the inducing field.

Lilley and Sloane (1976) applied the derivatives of the field technique to find conductivity-structure under 1-D cases. The frequency dependent conductivity response $C(\omega, k)$ when the field is non-uniform can be written as:

$$C(\omega, k) = \frac{\partial Z}{\frac{\partial X}{\partial x} + \frac{\partial Y}{\partial y}}$$

where $k = k_x^2 + k_y^2$. k_x & k_y being the wave numbers of the incident field in x- and y-directions. Lilley and Sloane derived the spatial gradients ($\partial X/\partial x + \partial Y/\partial y$) from Fourier maps of X and Y. This was done by fitting second order surface to the field in form of equation:

$$X = a_0 + a_1 x + a_2 y + a_3 x^2 + a_4 y^2 + a_5 xy$$

A second order surface is useful in the sense that it removes second order effects even though the second-order derivative does not appear in estimation of $C(\omega, k)$. Knowing $C(\omega, k)$ the apparent resistivity and depth of the conductor can be obtained from the relationships:

$$\rho_a = \omega \mu_0 |C_{imag}(\omega, k)|^2$$

$$\text{Actual depth} = h^* + \delta/2$$

where $h^* = C_{real}(\omega, k)$ and δ = skin depth.

The apparent resistivity obtained for the Australian region is shown in Fig. 8. The analysis was done for Sq variations. Over Australian region, near the Sq-focus, the variation becomes spatially non-uniform with non-zero first derivative. The conductivity estimates of Lilley and Sloane are in close agreement with global average.

(V) Global Conductivity Distribution

Variation of conductivity inside the earth has been estimated through geomagnetic data by several workers. Lahiri and Price were the first one to attempt this. A look for model the density distribution inside earth as

$$\sigma = \sigma_0 \left(\frac{r}{R_E}\right)^{-l}.$$

The three model parameters σ_0, R_E and l were estimated by making a fit to observed H and Z-variations over the earth's surface. Lahiri and Price used Sq and storm-time variations. R_E was found to be ~~little~~ less than the radius of the Earth. This line of research has continued since then. Later workers included 27-day, 13.5-day, 9-day, 6-month and 12-month periodicity also. The distribution reported by some of the workers is given in Fig. 9. All models contain a sharp increase in conductivity at a depth of about

600 km. This gives rise to the concept of conducto-sphere. In the figure we have also shown by dotted lines, the distribution under ~~in~~ ocean floor. Main difference between oceanic and Continental profiles seems to be that the increase in conductivity occurs at a much shallower depth under oceans. It is also found that the conducting layer is shallower at the younger sea floors.

References

B. R. Arora, 1987. Phys. Earth & Planet Interiors.

Sharmila Banerji et al, Annales Geophysicae, 1986, 4, 529-536

Dimitrev V.I. and Bondichansky M.N., 1979. Proc. IEEE, 67, 1034-1043.

Wait, J.R., 1954, Geophysics, 19, 281-289.

Lilley, F.E.M. and Sloane, M.N., 1976. J. Geomagn. Geoelect., 28, 321-328

Lilley, F.E.M., Woods, D.V. and Sloane, M.N., 1981, Phys. Earth Planet Int., 25, 232-240.

Some Important References

MV Studies:

Reviews

Hutton, V.R.S., 1976. Rep. Progress in Ph
39, 487-572.

Singh, B.P., 1980, Geophysical Surv
4, 71-87

Alabi, A.O., 1983, Geophysical Surv
6, 153-172.

Many of the important papers are cited in these three references.

MT fluids

Sims, W.E and Bostick, Jr, F.X., 1969.
University of Texas at Austin,
Electronics Research Center Report,
No. 58.

Vozoff, K., 1972, Geophysics, 37, 98-141.

Pedersen, J. and Haremoës, I.F., 1986,
Surveys in Geophysics, 8, 187-231.

Jones, F.W. and Pascoe, L.J., 1971, Geophys
J. Roy. Astron. Soc., 20, 317-334

Cagniard, L., 1953, Geophysics, 18, 605-635.

Bostick, F.X., Jr., 1977. Univ. of UTAH Rep.

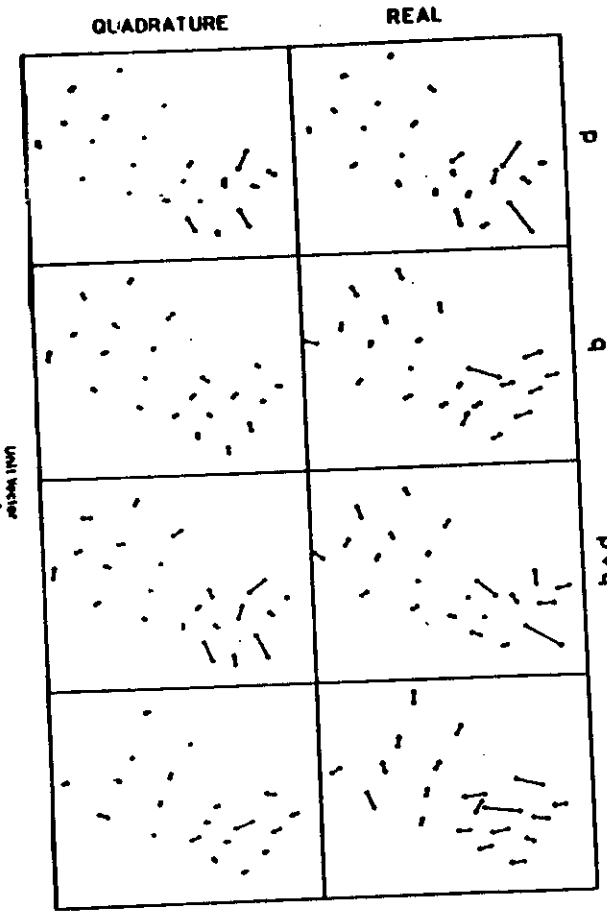

Fig. 2. Real and quadrature parts of horizontal perturbation arrows, p, q, p + q, and induction (I) arrows for the stations of northwest

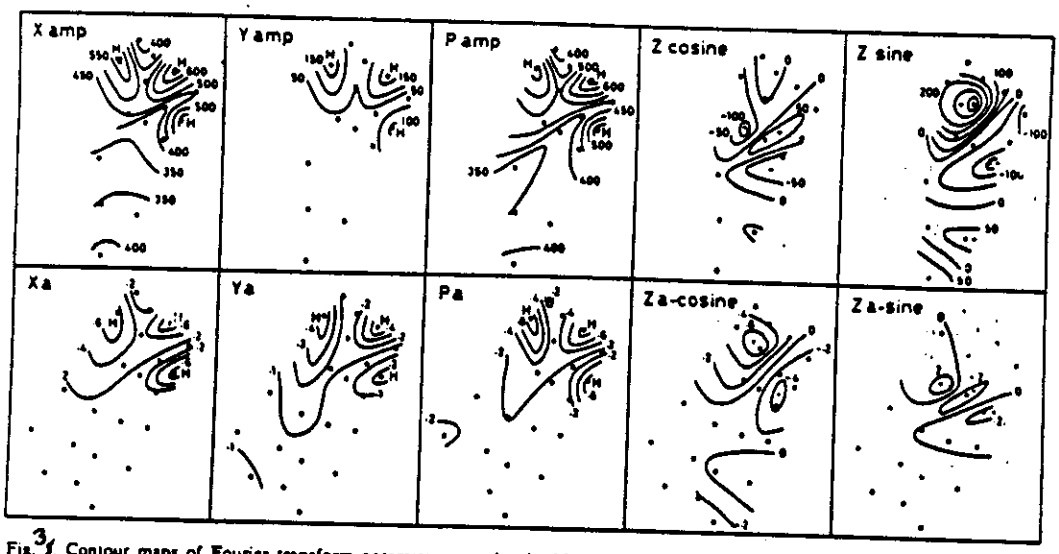

Fig. 3. Contour maps of Fourier transform parameters associated with north polarized horizontal field at 39 min period (upper panel). The lower panel gives the simulated anomalous field for similarly polarized horizontal field of unit amplitude. Simulated maps are for a 41 min period.

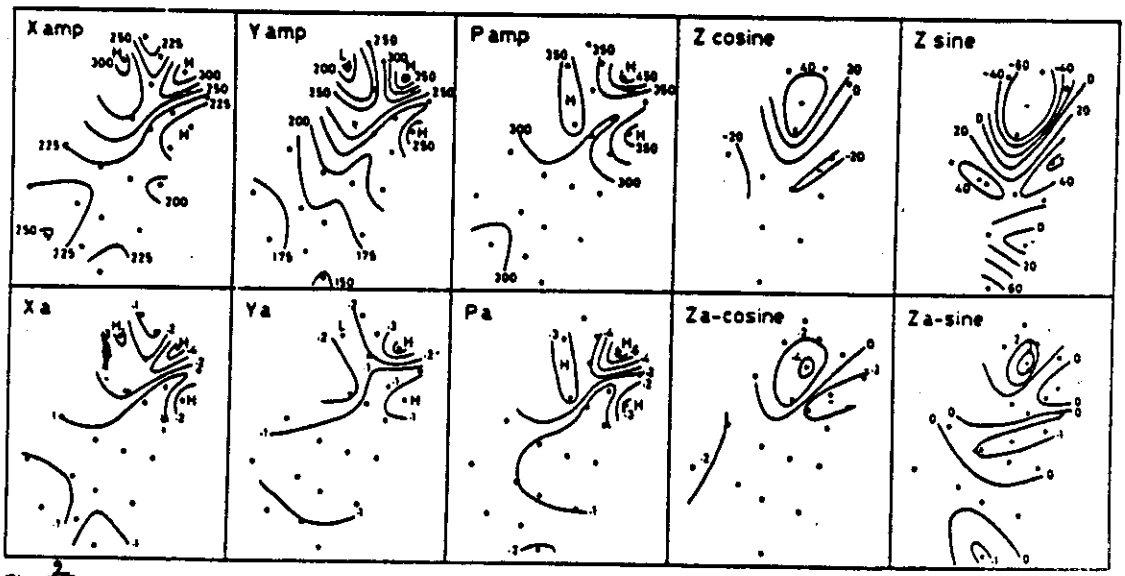

Fig. 4. Contour maps of Fourier transform parameters associated with a northwest polarized horizontal field at 91 min period (upper panel). The lower panel gives the simulated anomalous fields maps for similarly horizontal field of unit amplitude.

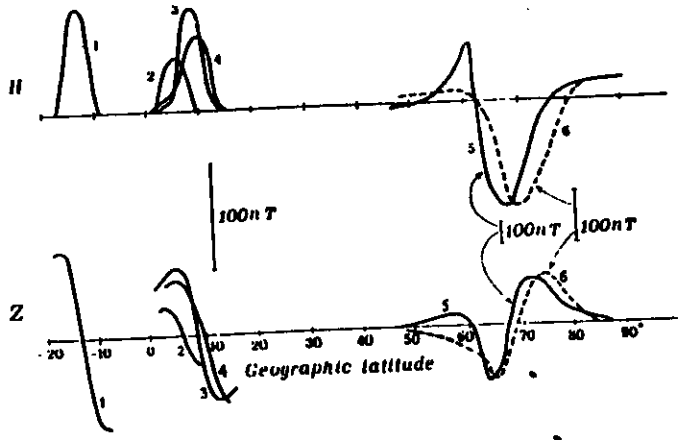

Fig. 4. The latitude dependence of the variations of *H*- and *Z*-components for the equatorial and auroral electrojet (scale is the same for *H* and *Z*). Data used: *1* Peru (Forbush and Casaverde 1961), *2* Nigeria (Onwumechilli 1967), *3* Central Africa (Fambitakoye 1973), *4* Chad (Godivier and Grenn 1965), *5* Canada (Walker 1964), *6* Scandinavia (Bonnevier et al. 1970)

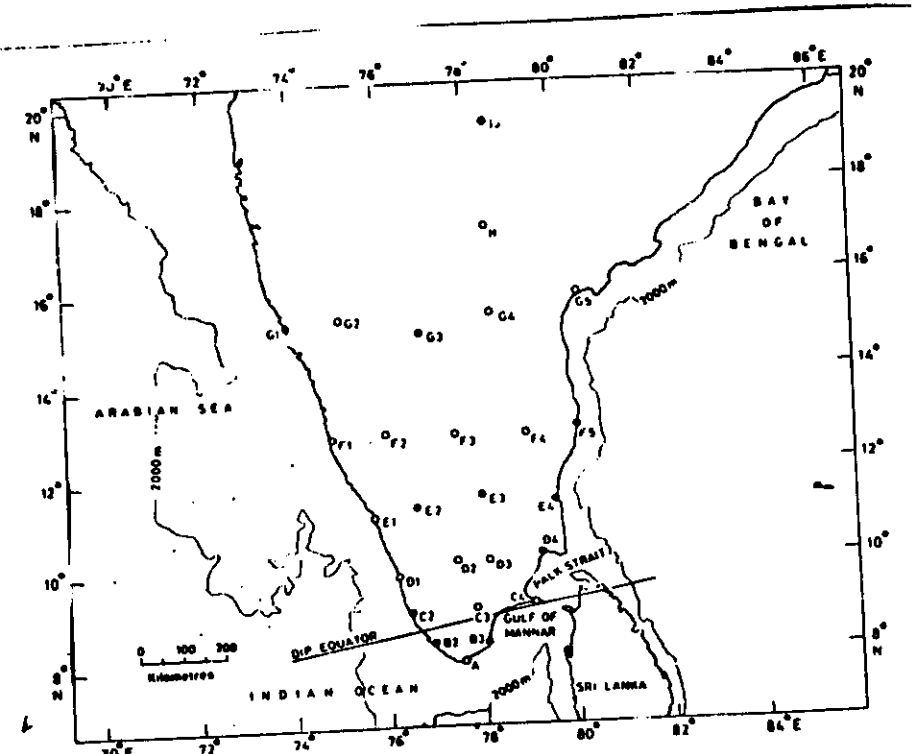

Figure 5
Map showing locations of magnetometer array stations in peninsular India. Filled circles indicate stations whose data are used in the present study.

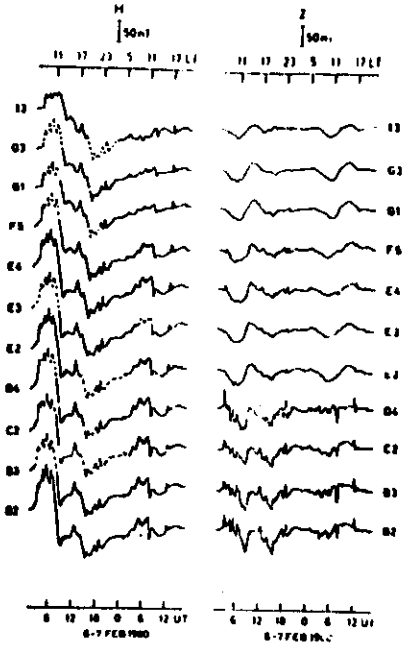

Figure 16
Storm time variations in horizontal (H) and vertical (Z) components at magnetometer array stations. Broken portion of the curves represents interpolated values because of the loss of data.

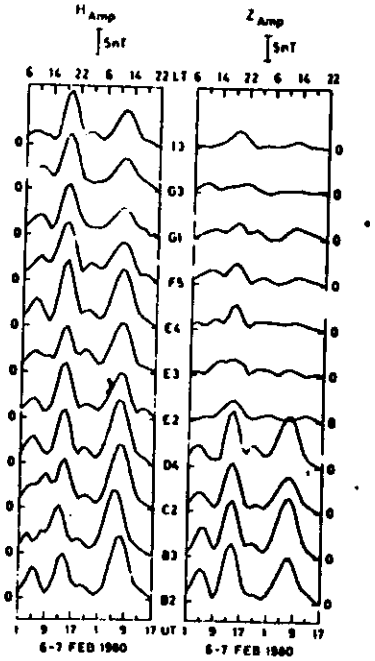

Figure 17
Amplitude demodulates of horizontal (H) and vertical (Z) components of geomagnetic field variations corresponding to period band of 171-82 min, during the magnetic storm of February 6-7, 1980.

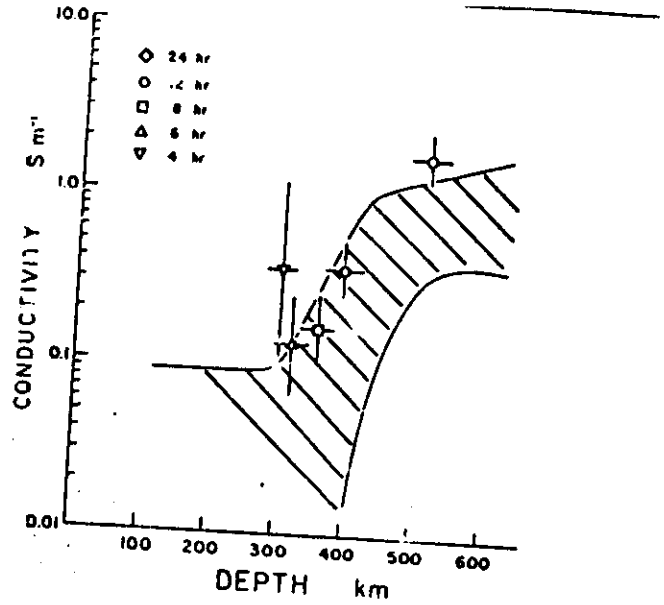

8
Fig 7. Conductivity versus depth from inversion of $C(w, k)$ at the principal periods of the Sq daily variation (from Lilley and Woods, 1979). The envelope encloses the upper and lower Limits of Banks (1969) best fitting model).

R. J. Banks, Geophys. J. Roy. Astron. Soc., 1975, 43, 87-101

Agarwal et al., Proc. Ind. Acad. Sci (Earth Planet Sci), 1979, 89, 67-77.

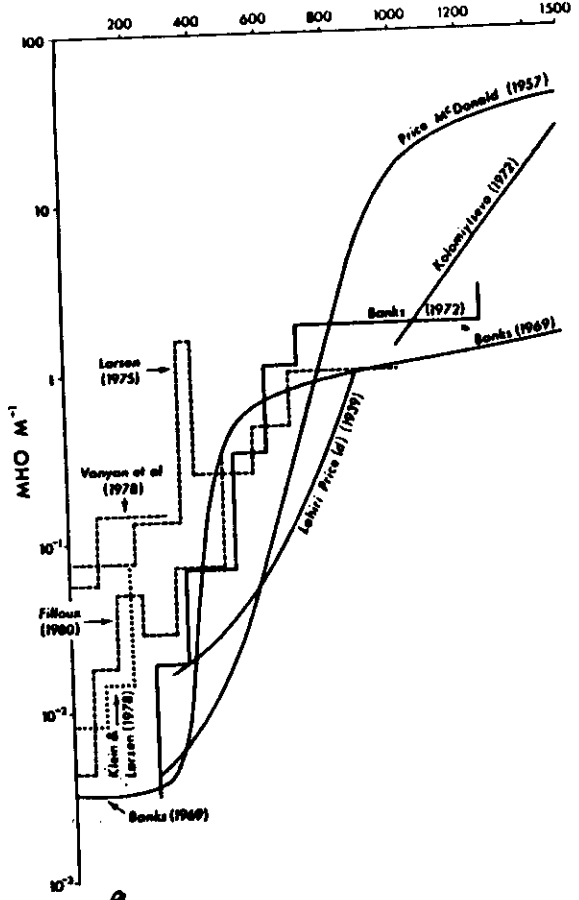

FIG. 1.12. Estimates of conductivity as a function of depth. Solid lines refer to continental measurements, dashed or dotted lines to ocean floor or ocean island measurements.

$\sigma = \sigma_0 \left(\frac{R}{a}\right)^{-1}$